IECB 2022

MDPI

Proceeding Paper

Sensitivity of the Au Cluster Attached to Graphene Nanopore in a SERS Sensor to Characterize Vibrational Spectra of Nucleotides †

Tatiana Zolotoukhina *, Mohd Aidil Amin Bin Mohd Nasir and Hiroki Yoshimizu

Department of Mechanical Engineering, University of Toyama, Toyama 930-8555, Japan; email1@gmail.com (M.A.A.B.M.); email2@gmail.com (H.Y.)

* Correspondence: zolotu@eng.u-toyama.ac.jp; Tel.: +81-76-445-6739

† Presented at the 2nd International Electronic Conference on Biosensors (IECB), 14–18 February 2022; Available online: https://iecb2022.sciforum.net/.

Abstract: The photochemical techniques applied to the sensing of bioactive molecules have become one of the fastest-growing scientific fields. Surface-enhanced Raman scattering (SERS) measurement is highly sensitive for detecting low-concentration; single molecules or oligomers, including DNA, microRNA, and proteins. In the field of SERS biosensor design, the use of carbon-based nanomaterials as substrate materials is rapidly developing, and we intend to investigate mechanisms of the dynamic interaction of oligomers with the environment of the SERS sensor to specify the fingerprints of such interactions in the spectra to enhance resolution. We study the vibrational spectra of the nucleotides in the dynamic interaction with the Au nanoparticles (NP) relaxed at (grown on) graphene nanopore that combines (1) translocation localization by graphene nanopore and (2) nucleotide interaction enhancement by Au NP. The spectral map of the cytosine nucleotide was tested by molecular dynamics (MD) simulation with LJ interaction between components. The spectra of various bonds were compared in reaction coordinates for DNA nucleotides and Cartesian ones for Au NP. Spectra at the interaction with the Au NP were used to select a transient COM velocity of nucleotide passing along the cluster. At the edge of the graphene pore, the velocity has been set at 0.025 m/s that compared with the experimental range. We test the sensor's system to evaluate the influence of the interaction with Au NP and graphene on the transient spectra calculated by MD. The frequencies and modes that can serve as markers of the corresponding Au—nucleotide and graphene—nucleotide interactions are estimated. The MD simulation creates spectral libraries for oligomer's vibrations to specify the interaction's type and strength in SERS sensors that can be further utilized as training data for the machine learning application in spectral recognition

Keywords: vibrational spectra; molecular dynamics; nucleotides; Au nanoparticle; SERS

Citation: Zolotoukhina, T.; Nasir, M.A.A.B.M.; Yoshimizu, H. Sensitivity of the Au Cluster Attached to Graphene Nanopore in a SERS Sensor to Characterize Vibrational Spectra of Nucleotides. **2022**, *4*, x. https://doi.org/10.3390/xxxxx

Published: date

1. Introduction

Development of new sensing methods for such single molecules as DNA, RNA, and proteins is essential for the accurate diagnosis of human disease that presently often requires time-consuming and expensive biomedical testing because relatively simple bioanalytical tests typically suffer from low sensitivity and selectivity and require large sample volumes for the analysis. Surface enhanced and tip-enhanced Raman spectroscopy (SERS & TERS) has advanced significantly to nanoscale resolution [1–9] and now has the potential to overcome microarray and qPCR limitations while maintaining its high sensitivity. The SERS ability to detect a single molecule [10,11] has been proven when the molecule has been deposited on colloidal metal or a substrate surface [12]. At the described conditions the method offers high molecular specificity [13]. In SERS, the Raman signal of adsorbed molecules is amplified at "hot spots" on the substrates surface [14]. Attention to

DNA/RNA and protein molecules in the manifold of applications makes identification of oligomers in a variety of states and interaction environments highly desirable in the non-contact real-time way of nanophotonic vibrational spectroscopy.

A two-step process of protein detection at a single molecule level using SERS was developed [15,16] as a proof-of-concept platform. The detection method has a protein molecule bound to a linker in the bulk solution and then chemically reacted with the SERS substrate and immobilized. Samples showed the typical behavior of a single molecule SERS including spectral fluctuations, blinking and Raman signal being generated from only selected points on the substrate.

Another path to the identification of small organic molecules, such as oligomers, has employed interaction with a nanopore in a 2D material's membrane, especially graphene [17–23] and hexagonal BN [24–27]. The detection of the following DNA/RNA oligomers, mononucleotides [28–30] and nucleobases [31], with SERS techniques has been demonstrated.

In the present roadmaps for single-molecule SERS spectroscopy [32,33], the experimental evidences of single-molecule SERS include intensity fluctuation as one of the representative evidences. The migration of surface atoms of SERS substrates (e.g., amorphous Au substrates) can influence the measured single-molecule signal. In single-molecule SERS using plasmonic metal nanoparticles, ultrahigh Raman enhancement has been achieved with plasmonic sharp tips as another type of configuration. The sharp geometric configuration is capable of realizing high concentration and localization of electromagnetic field in nanoparticles with sharp tips (e.g., sea-urchin-like nanoparticles) [34]. Another technique based on the plasmonic sharp tips is tip-enhanced Raman spectroscopy (TERS) and has a shifting precision of subnanometer. TERS, as an extension technique of SERS, not only provides a single-molecule sensitivity but also enables Raman measurement in space domain with a subnanometer resolution.

In order to design and simulate the sensor that would let single oligomer detection, the 2D graphene as substrate is combined with a sharp configuration Au nanoparticle (NP) localized at the edge of nanopore. Such design let to guide the single oligomer through the created "hot" spot. [35,36] We intend to simulate by molecular dynamics (MD) method the mechanisms of the dynamic interaction of oligomers with the environment of the SERS sensor to specify the fingerprints of such interactions in the spectra of each component of the nucleotide-AuNP-graphene system to enhance resolution. We study the vibrational spectra of the nucleotides in the dynamic interaction with the Au nanoparticles (NP) relaxed at (grown on) graphene nanopore that combines (1) translocation localization by graphene nanopore and (2) nucleotide interaction enhancement by Au NP. The spectral map of the cytosine nucleotide was obtained by molecular dynamics (MD) simulation with the Van der Waals (LJ) interaction between components. The spectra of various bonds were calculated in reaction coordinates for cytosine as the sample oligomer and Cartesian coordinates for Au NP and graphene. Spectra at the interaction with the Au NP were used to select a transient COM velocity of nucleotide passing along the cluster. At the edge of the graphene pore, the velocity has been set at 0.025 m/s that compared with the experimental range. We study the sensor's system to evaluate the influence of the interaction with Au NP and graphene on the transient spectra calculated by MD. The frequencies and modes that can serve as markers of the corresponding Au—nucleotide and graphene—nucleotide interactions are estimated. The MD simulation can creates spectral libraries for oligomer's vibrations to specify the interaction's type and strength in SERS sensors that can be further utilized as training data for the machine learning application in spectral recognition.

2. Model and Methods

The present study considers the nucleotide-Au NP-graphene system simulation by the MD method to evaluate the influence of the system components on the vibrational spectra of each part. The nucleotide vibrational frequencies we obtained in reaction

coordinates and they have been attributed to stretching, bending or ring-breathing modes. The vibrational frequencies of the Au NP and graphene were calculated in the Cartesian coordinates for each atom selected to reflect the effect of component's interaction. The vibrational density of states is calculated in the transient regime during passing time through the graphene nanopore for each atom in the bonds of the oligomer and selected atoms of the Au NP and graphene to resolve the difference in the spectra, structural and due to interaction. In dynamics, the vibrational spectra are being evaluated from MD propagation velocities computed in the anharmonic interaction potentials in the the components of the nucleotide-Au NP-graphene system, the LJ potential is used between components. Fourier transfer *I(f)* of the velocity autocorrelation function *G(τ)* is as follows

$$G(\tau) = \frac{<v_i(t_0) \cdot v_i(t_0+\tau)>}{<v_i(t_0) \cdot v_i(t_0)>} \quad , \qquad I(f) = \int_{-\infty}^{\infty} G(\tau) \exp(-2\pi i f t) d\tau \tag{1}$$

where τ is the duration of correlation, $v_i(t_0)$ is the velocity of the atom at time t_0, and $v_i(t_0 + \tau)$ is the velocity of the atom during correlation time. According to Wiener-Khinchin theorem, $I(f)$ defines the vibrational density of states (DOS) of the system. The potential used for DNA nucleotides is MM2/MM3 force field potential [37]. We investigate the transient interaction with graphene modelled by REBO potential [38], Au NP modelled by EAM potential [39,40] and the molecule-graphene interaction for C-X (X = H, O, C, N) by the LJ potential [37]. The interaction causes a shift in some frequencies of vibrations of the nucleotide DOSes. The vibrational spectra in MD exhibit shifts and intensity changes due to interaction between system components that causes inter-component and intramolecular vibrational mode dynamics.

The principal SERS sensor design and subsequent calculation setup is presented in Figure 1.

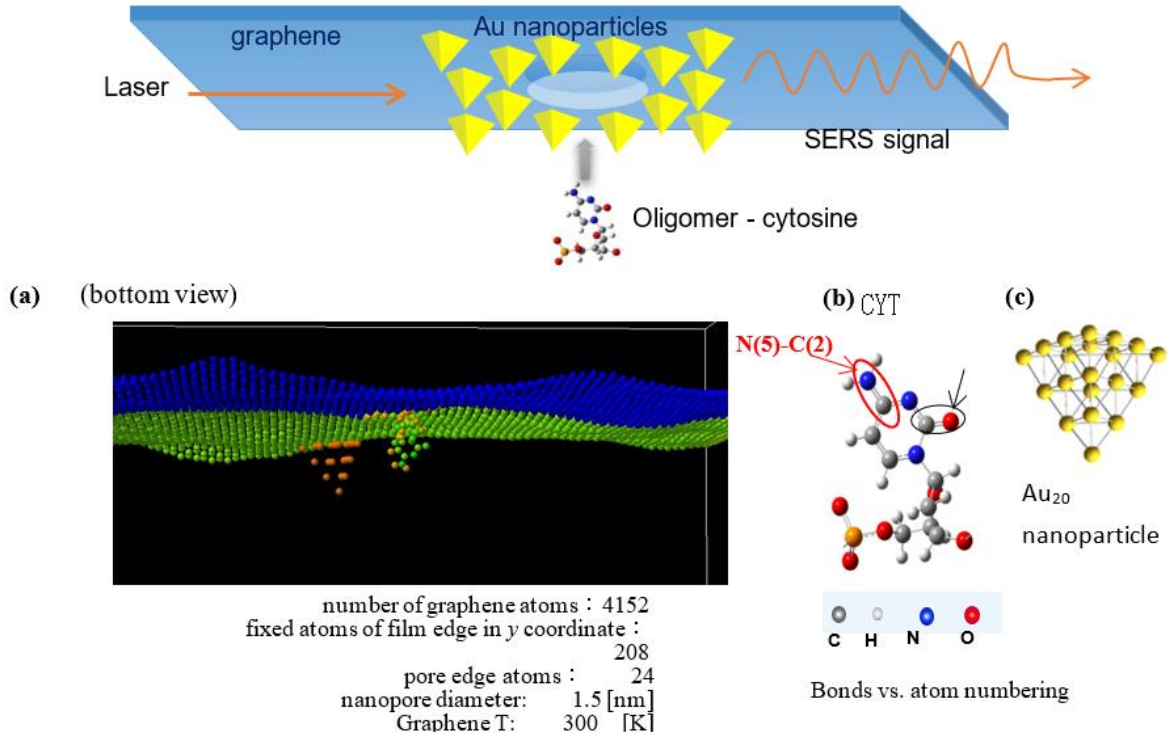

Figure 1. The principal SERS sensor design. (**a**) The structure and translocation position of cytosine nucleotide inside of the graphene pore. The spatial orientation of the nucleotide's cyclic plane is at 30° to the z-x plane. Atoms are shown: C in grey, N in blue, O in red, and H in light grey. (**b**) Initial

configuration of cytosine (right) is shown on the left with an example of corresponding atom numbering for bonds in MD calculations. (**c**) Optimized by DFT GGA calculations Au_{20} nanoparticle.

To the graphene sheet with the 1.5 nm in diameter pore at its center is attached the Au_{20} NP in the pyramidal shape at the edge of the pore. A location of the cytosine that is selected as the tested oligomer relative to the pore plane and center is shown in the process of translocation in the pore. The graphene sheet is oriented in the x-y-plane, the edges along the *y*-axis are fixed, and the edges along the *x*-axis are free. The nucleotide can move with a given added velocity of the center of mass ($v_{c.o.m.}$) in the positive z-direction that overall reproduces the motion in a constant electric field in experimental setups. All atoms of the system except fixed ones are thermally relaxed before sampling to the temperatures $T_{graphene}$ = 300 K and $T_{nucleotide}$ = 30 °C, as marked in Figure 1. The Au NP is initially placed at the 4 Å distance from cytosine nucleotide that maximizes the Van der Waals interaction between the NP and the molecule without the nucleotide sticking to the surface of the NP as shown in Figure 2. In the next step, the Au NP is lifted to the graphene surface close to the pore edge. The distance was selected with regards to results on diffusion of gold nanoclusters on graphite [41]. LJ interaction potential between Au NP and graphene was set with σ(C-Au) = 2.74 A and ε(C-Au) = 0.022 eV = 3.524788×10^{-21} J, truncated at 4.50 Å [41]. The two attachment distances were tested (see Figure 2) and it was found that $R_{Au\text{-}C}$ = 3.05 Å gives a stable dynamics of the graphene—Au NP system while 2.45 Å destroys the pore edge in MD simulation. COM velocity of the AuNP has been initially kept equal 0 m/s at the time of calculation. However, as it might affect the pore edge graphene atom's dynamic and interaction, the Au NP was relaxed relative to the graphene prior to sampling and remained unrestricted in the production run. In the translocation process, the single layer graphene sheet with attached NP interacts with the nucleotide in graphene nanopore. Graphene and Au NP affect the interaction field of the passing oligomer close to the pore edge. The graphene-molecule C-X (X = H, O, N, C) and Au-X (X = H, O, N, C) potentials are considered as a VdW ones to avoid bond creation and nucleotide attachment in the pore.

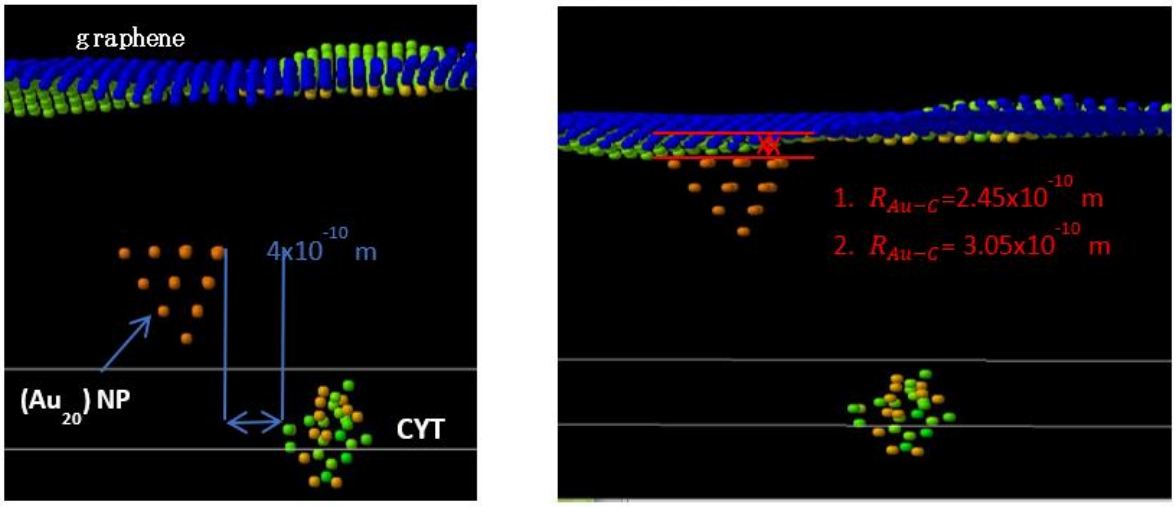

Figure 2. Distance between Au NP and cytosine at the left panel, distance between Au NP and graphene sheet at the right panel. Distances are selected to maximize Van der Waals interaction.

The transient MD calculations are sensitive to the duration of correlation time and relative interaction of the structures studied. As was shown in [35,36], the time step of 0.05 fsec and 32,768 step number reach the resolution of vibrational modes being Δf = 20 cm^{-1} and frequency interval being up to 4000 cm^{-1}. The Δf = 20 cm^{-1} spectral resolution is comparable to the 15 cm^{-1} half-width of Lorentzian function that is used to broaden Raman spectral lines in DFT calculation [42]. The assumed resolution introduce low level

"shadow" frequencies from adjacent bonds, therefore, only highest peaks in the spectrum are considered as modes. Interaction and conformation dependent single molecule calculations collect correlation data on the time scale of few vibrational periods that are presently covered with 1.64 psec time interval. That approaches the psec timescale of nanophotonic probing of the acoustic phonon propagation [43]. The employed spectral resolution in our MD calculations has been sufficient to register structural and interaction dependence of the spectral map of all 3 components of the system which were treated at the same resolution.

3. Results

In the current study, we estimated in several steps optimal simulation setup of the nucleotide—Au NP—graphene system. As the first step, the translocation velocity of the oligomer has been tested versus possible spectral changes at the interaction with Au NP. The next step was to lift and attach the Au NP to graphene and relax the graphene—Au NP part of the system. Then, we tested spectra of system components to extract influence of the interaction between the components on the component's spectra.

3.1. Velocity of Oligomer Translocation

Considering the DNA translocation velocity, experimental results in aqueous solution [44,45] give the range of the velocity to be in the 0.1–0.01 m/s interval. The nucleotide's v_{COM} is tested for the following values 0.02, 0.025, 0.03 m/s that were optimized to enhance the interaction force between the nucleotide and edge of graphene pore and reduce rotation of the nucleotide in the translocation as much as possible. From simulation, we estimate that the optimum center of mass' velocity for cytosine (CYT) is around 0.025 m/s. To confirm our estimation, we compare the interaction period of CYT and Au NP and vibrational spectra with +–0.05m/s velocity changes. The result obtained can resolve nucleotide's interaction with each Au NP and graphene, however, calculated spectra were collected for detached Au NP only to compare spectral response to v_{COM} for the single interaction with Au NP (as shown in Figure 2, left panel, 12 Å from the graphene sheet) with exclusion of graphene. There is bending and twisting at 500 [cm^{-1}]–1000 [cm^{-1}] interval seen in Figure 3c,d, and some modes have amplitude changes. An amplitude changes of several to 30% was observed in the 1200–2000 [cm^{-1}] range, responsible for the C-X (X = C, N, O) stretch modes. For the stretching modes of the hydrogen bonds C-H & N-H, the stretching modes in the [2400–3500] range have up to 50% change in the amplitude for v_{COM} change from 0.02 m/s to 0.03 m/s. The cytosine spectra remain stable relative to the variations in the translocation velocity of the nucleotide up to 30% in present calculations. Additional data on the distance between Au_{20} cluster and CYT in x, y, z directions and velocity during translocation can be found in Figure A1 of Appendix A.

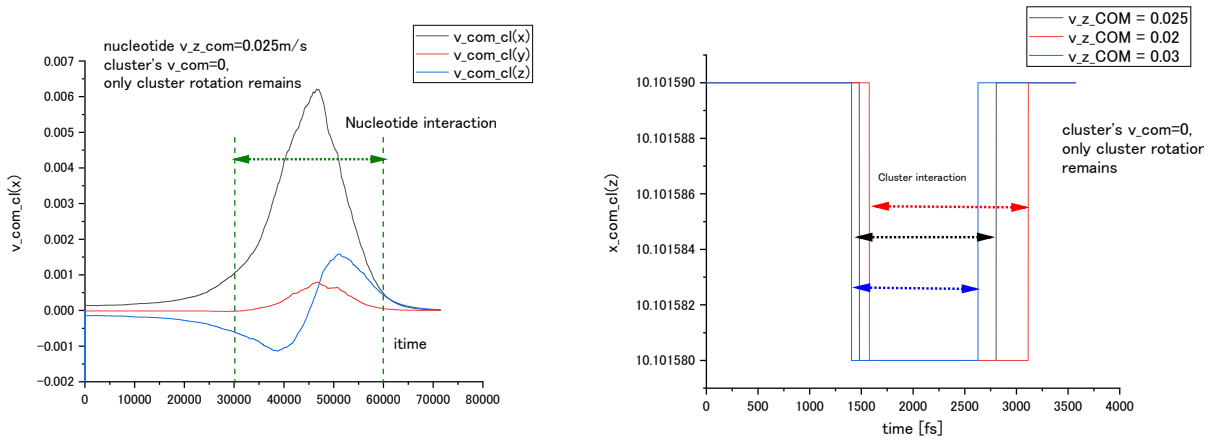

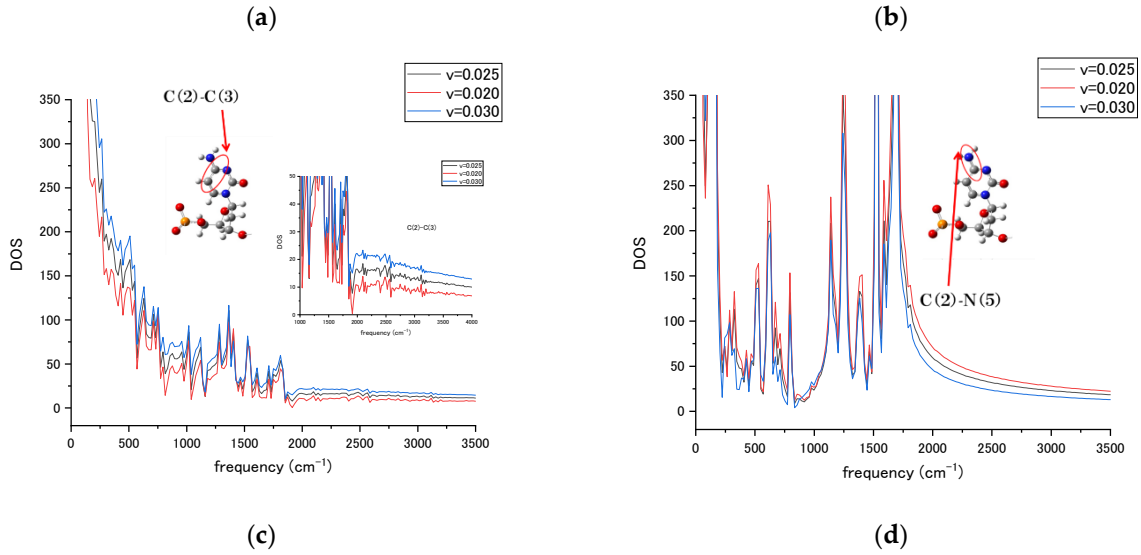

Figure 3. (**a**) The Au NP response to interaction with CYT by changes in the v_{COM} of NP relative to time steps, (**b**) the $x_{c.o.m}$ of NP relative to time registers the duration of interaction, (**c**) spectrum of cytosine C(2)–C(3) bond at different velocities of v_{COM} of Au NP, (**d**) spectrum of cytosine C(2)–N(5) bond at different velocities of v_{COM}. AuNP upper plane' distance to graphene is 12 Å.

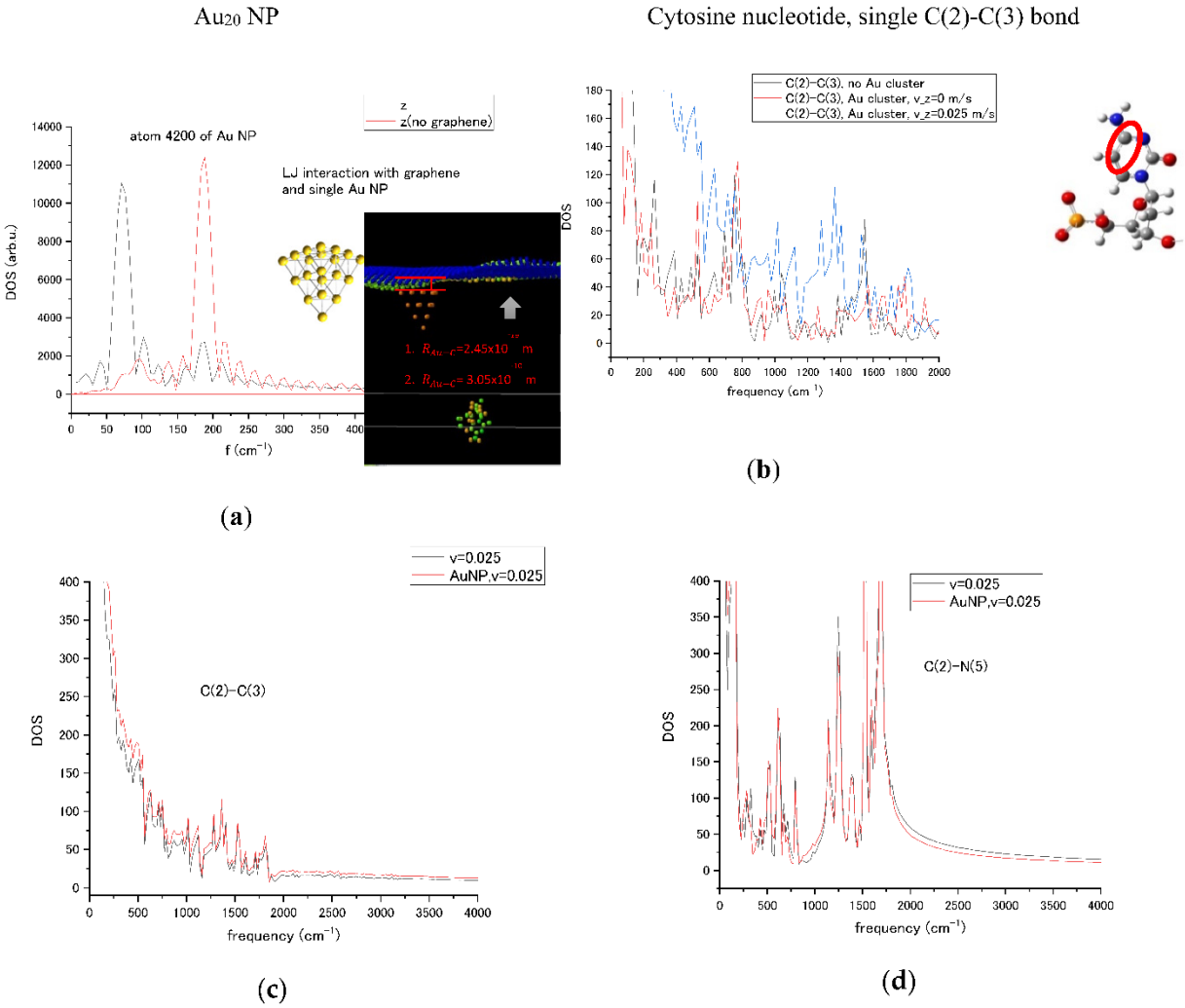

Figure 4. (**a**) Vibrational spectra of the 4200 atom of Au$_{20}$ nanoparticle attached to graphene in z direction with and without graphene; (**b**) cytosine C(2)-C(3) ring bond marked on the right panel;

(**c**,**d**) cytosine C(2)-C(3) and C(2)-N(5) vibrational spectra's comparison with Au NP absent and present moving with $v_{COM}(z) = 0\ and\ 0.025\ m/s$ with no interaction with graphene included.

3.2. Spectral Response to Interaction by System Components

The vibrational spectra of the nucleotides in the dynamic interaction with the Au NP attached by Van der Waals interaction to the edge of graphene nanopore (Figure 2, right pane) compared with the spectra for nucleotides passing by Au NP only (Figure 2, right pane) to reveal the spectral changes. In Figure 5, two types of spectral response on the presence of the interaction with graphene are shown. The bonds with attached H or NH_2 exhibit changes in the modes attributed to the C-C stretching, ring breathing, and NH_2 bending. The ring modes with frequencies of 1526 cm^{-1} and 1404 cm^{-1} present at all types of interaction, however, Van der Waals interaction of H with graphene pore edge excites additional modes shown in black in Figure 5a. The bond without attachment to the H remains almost unchanged by interaction with graphene at the translocation with $v_{COM}(z) = 0.025\ m/s$ through the pore.

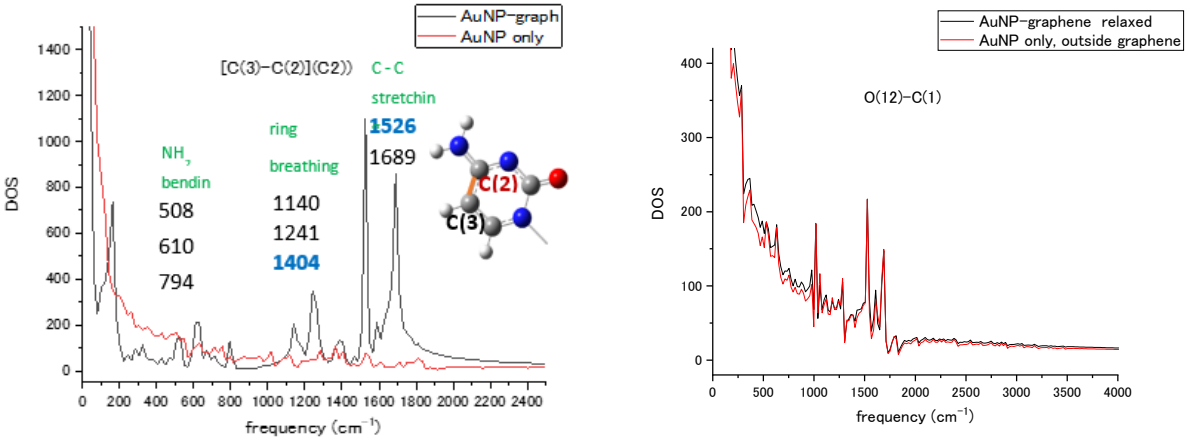

(**a**) (**b**)

Figure 5. Reaction of the vibration on the interaction with graphene for the bonds: (**a**) C(3)-C(2) from the C(2) side has spectral differences in frequencies marked in black for graphene only case and in blue for modes present in both cases; (**b**) O(12)-C(1) bond exhibits almost no differences in spectra.

We also registered the vibrational spectra of selected individual graphene atoms in order to reflect changes induced by interaction with nucleotide (Figure 6) as well as interaction with attached Au NP (Figure 7). Interaction with cytosine causes number of splitting and shifts in the bending modes of graphene atoms in x and y directions. Spectra in z direction register low frequency's vibration of the graphene sheet and its pore edge that are partially suppressed by interaction with the nucleotide. The interaction of graphene with attached Au NP is traced in spectra of Figure 7. The edge atom 2176 shows essential changes in the in-plane (x & y direction) modes as compared with the changes in Figure 6 that separate changes in spectra of graphene's pore edge atoms related to the oligomer translocation. As can be seen from the Figure 7d data, the out-of-plane modes exhibit signature 3 peaks starting from 427 cm^{-1} frequency that tag presence of the Au NP below the graphene surface. Changes in the in-plane modes (Figure 7b,c) are much more numerous as compared with the Figure 6b,c. Not only G mode localized for the edge atoms at vicinity of 1800 cm^{-1} in the present MD calculation is affected by presence of the Au NP but for pore edge atom 2176 lower frequency mode changes have the amplitudes enhanced with either the red shift or splitting of some modes.

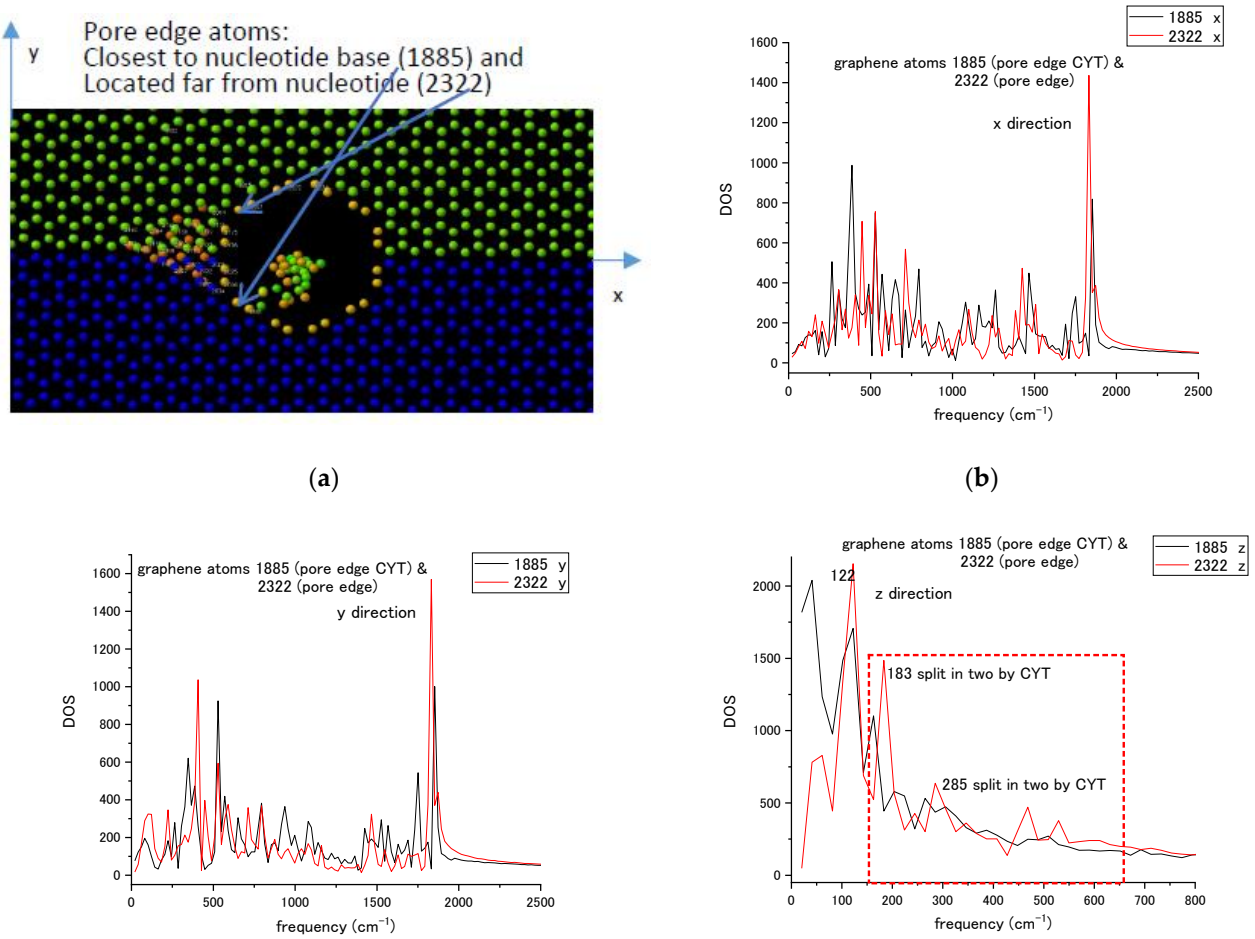

Figure 6. (**a**) Graphene pore edge atoms marked a 2322 and 1885 next to cytosine nucleotide; (**b**) the spectra in *x* velocity component; (**c**) the spectra in *y* velocity component; (**d**) the spectra in *z* velocity component.

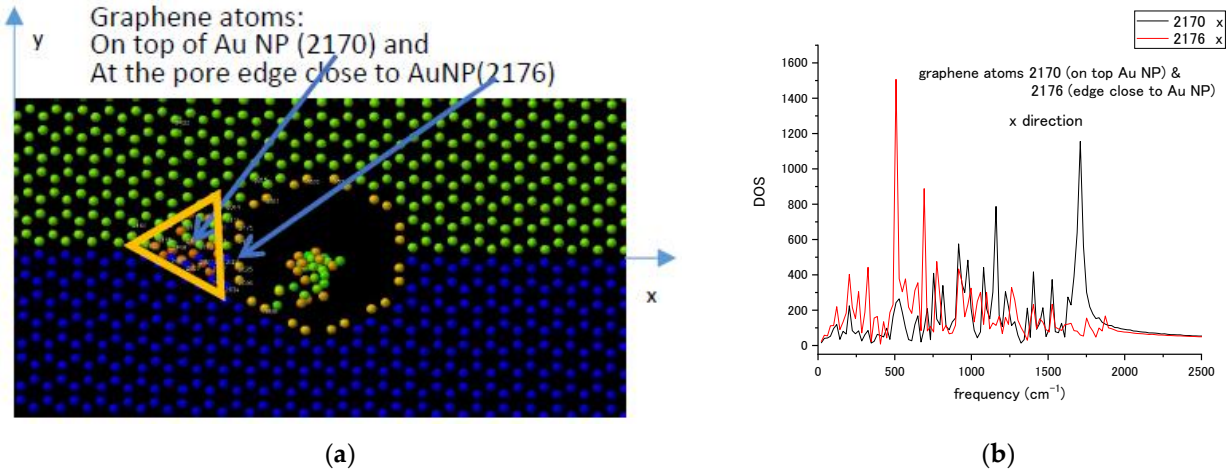

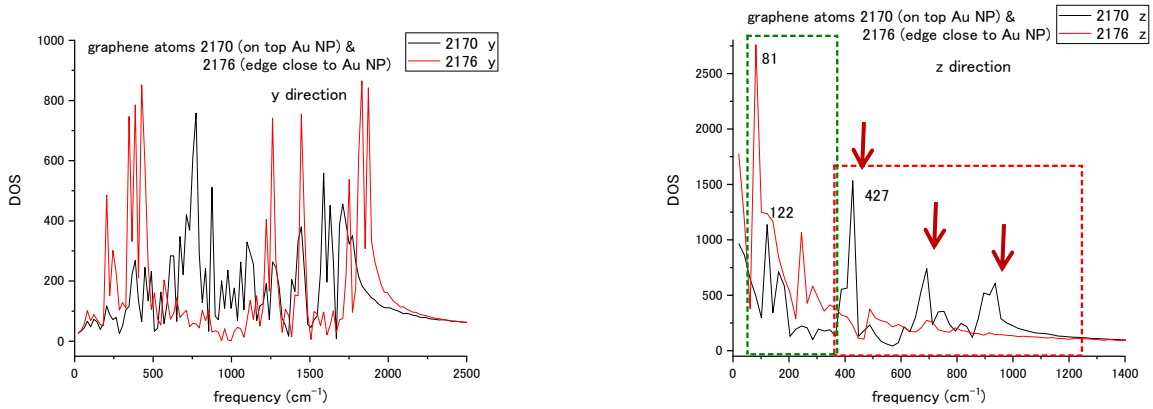

(**c**) (**d**)

Figure 7. (**a**) Graphene atom atop of Au NP marked as 2170 and at the pore edge 2176 next Au NP; (**b**) the spectra in x velocity component; (**c**) the spectra in y velocity component; (**d**) the spectra in z velocity component.

The task to separate probable contributions into evaluated spectral maps of translocating oligomers from system components is a multicomponent one. The present research gives an overview of vibrational spectral changes corresponding to particular parts of the interaction in the system of oligomer—Au NP—graphene nanopore. The knowledge of spectral changes in the graphene and Au NP modes at the time of oligomer translocation can serve as an additional marker of interaction and localization of a particular measured oligomer in the system. From experimental point, SERS intensity fluctuation is one of the representative experimental evidences of single-molecule SERS. The fluctuation is related to the instability of surfaces of SERS substrates. The measured single-molecule signal can be influenced by the migration of surface atoms of SERS substrates (e.g., amorphous Au substrates). The knowledge of spectral characteristics of the substrate at different configurations will be able to resolve possible fluctuations of the SERS signal in the sensor.

4. Discussion

The study of the vibrational spectra of the nucleotides in the dynamic interaction with the Au nanoparticles (NP) located at the surface of graphene next to the nanopore can't be considered complete without the investigation of the scope of changes in vibrational spectra of surrounding components of the system included into interaction. We confirm the oligomer interaction enhancement by Au NP and graphene. The obtained vibrational spectra are sensitive enough to reflect even weak Van der Waals interactions in each component of the system studied. Therefore, shape and size of Au NP and graphene pore will affect transient vibrational spectral maps of oligomers passing through the system. To calibrate and automate single molecule measurements, machine learning algorithms are ready to be utilized. The MD simulation creates spectral libraries for oligomer's vibrations to specify the interaction's type and strength in SERS sensors that can be further utilized as training data for the machine learning application in spectral recognition.

Author Contributions: Conceptualization, methodology, software development, validation, supervision T.Z.; data curation, M.A.A.B.M.N., H.Y.; writing—original draft preparation, review and editing, T.Z. All authors have read and agreed to the published version of the manuscript.

Funding: This research received no external funding.

Institutional Review Board Statement:

Informed Consent Statement:

Data Availability Statement:

Acknowledgments: T.Z. gratefully acknowledges the technical assistance in the calculations and preparation of the results of Appendix A done by H. Mizuguchi and T. Kitani. All calculations were performed at Applied Mechano-Informatics Laboratory in Toyama University.

Conflicts of Interest: The authors declare no conflict of interest.

Appendix A

The COM velocity of nucleotide is set at 0.025m/s while Au NP has velocity 0 m/s (Figure 2). Then, we compare the deviation in the distance between Au NP and cytosine shown in Figure A1a relative to the time step count. Changes in the nucleotide's COM velocity with time are traced in Figure A1b. With obtained data, the interaction time has been localized and used in the selection of the correlation time in Equation (1) for the particular set up of nucleotide translocation velocity and distance from the Au NP and graphene pore.

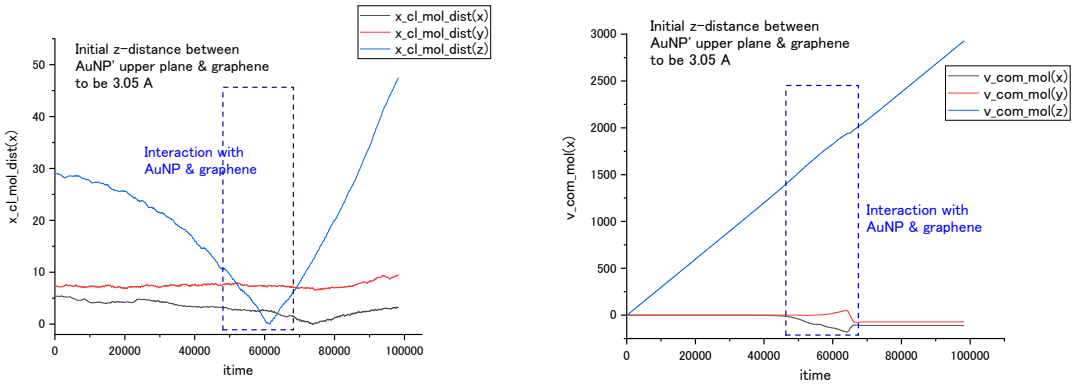

(**a**) (**b**)

Figure A1. (**a**) Distance between Au_{20} cluster and CYT in x, y, z directions; (**b**) cytosine`s center of mass velocity changes, v_x, v_y, v_z during propagation with $v_{COM}(z) = 0.025\ m/s$.

References

1. Han, X.X.; Rodriguez, R.S.; Haynes, C.L.; et al. *Nat. Rev. Methods Primers* **2022**, *1*, 87.
2. Stöckle, R.M.; Suh, Y.D.; Deckert, V.; Zenobi, R. *Chem. Phys. Lett.* **2000**, *318*, 131–136.
3. Hayazawa, N.; Inouye, Y.; Sekkat, Z.; Kawata, S. *Opt. Commun.* **2000**, *183*, 333–336.
4. Knoll, B.; Keilmann, F. *Nature* **1999**, *399*, 134–137.
5. Taubner, T.; Keilmann, F.; Hillenbrand, R. *Nano Lett.* **2004**, *4*, 1669–1672.
6. Zhu, Z.; Zhan, L.; Hou, C.; Wang, Z. *IEEE Photonics J.* **2012**, *4*, 1333–1339.
7. Anker, J.N.; Hall, W.P.; Lyandres, O.; Shah, N.C.; Zhao, J.; van Duyne, R.P. *Nat. Mater.* **2008**, *7*, 442–453.
8. Saha, K.; Agasti, S.S.; Li, C.K.X.N.; Rotello, V.M. *Chem. Rev.* **2012**, *112*, 2739–2779.
9. Guerrini, L.; Krpetic, Z.; van Lierop, D.; Alvarez-Puebla, R.A.; Graham, D. *Angew. Chem. Int. Ed.* **2015**, *54*, 1144–1148.
10. Kneipp, K.; Wang, Y.; Kneipp, H.; Perelman, L.T.; Itzkan, I.; Dasari, R.R.; Field, M.S. *Phys. Rev. Lett.* **1997**, *78*, 1667–1670.
11. Greve, C.; Elsaesser, T. *J. Phys. Chem. B* **2013**, *117*, 14009–14017.
12. Blackie, E.J.; le Ru, E.C.; Etchegoin, P.G. *J. Amer. Chem. Soc.* **2009**, *131*, 14466–14472.
13. Aydin, Ö.; Altaş, M.; M.; Kahraman; Bayrak, Ö.F.; Çulha, M. *App. Spectroscopy* **2009**, *63*, 1095–1100.
14. Ko, H.; Singamaneni, S.; Tsukruk, V.V. *Small* **2008**, *4*, 1576–1599.
15. Doyle, F.; et al. *Sci. Rep.* **2017**, *7*, 45393–45393.
16. Almehmadi, L.M.; Curley, S.M.; Tokranova, N.A.; et al. *Sci. Rep.* **2019**, *9*, 12356.
17. Li, J.; Gershow, M.; Golovchenko, J.A. *Nat. Mater.* **2003**, *2*, 611–615.
18. Yang, N.; Jiang, X. *Carbon* **2017**, *115*, 293–311.
19. Thompson, J.F.; Milos, P.M. *Genome Bio.* **2011**, *12*, 217.
20. Shankla, M.; Aksimentiev, A. *Nat. Commun.* 2014 **5**, 5171.
21. Liang, L.; Shen, J.-W.; Zhang, Z.; Wang, Q. *Biosens. and Bioelectron.* **2017**, *89*, 280–292.
22. Zhang, Z.; Shen, J.-W.; Wang, H.; Wang, Q.; Zhang, J.; Liang, L.; Ågren, H.; Tu, Y. *J. Phys. Chem. Lett.* **2014**, *5*, 1602–1607.
23. Liang, L.; Zhang, Z.; Shen, J.; Zhe, K.; Wang, Q.; Wu, T.; Ågren, H.; Tu, Y. *RSC Adv.* **2014**, *4*, 50494–50502.
24. Zhou, Z.; Hu, Y.; Wang, H.; Xu, Z.; Wang, W.; Bai, X.; Shan, X.; Lu, X. *Sci. Rep.* **2013**, *3*, 3287.

25. de Souza, F.A.L.; Amorim, R.G.; Scopel, W.L.; Scheicher, R.H. *Nanoscale* **2017**, *9*, 2207–2212.
26. Zhang, L.; Wang, X. *Nanomaterials* **2016**, *6*, 111.
27. Gilbert, S.M.; Dunn, G.; Azizi, A.; Pham, T.; Shevitski, B.; Dimitrov, E.; Liu, S.; Aloni, S.; Zettl, A. *Sci. Rep.* **2017**, *7*, 15096.
28. Lee, D.; Lee, S.; Seong, G.H.; Choo, J.; Lee, E.K.; Gweon, D.-G.; Lee, S. *App. Spectroscopy*, 2006, **60**, 322A.
29. Bell, S.E.J.; Sirimuthu, N.M.S. *J. Am. Chem. Soc.* **2006**, *128*, 15580–15581.
30. Madzharova, F.; Heiner, Z.; Gühlke, M.; Kneipp, J. *J. Phys. Chem. C* **2016**, *120*, 15415–15423.
31. Chen, C.; Li, Y.; Kerman, S.; Neutens, P.; Willems, K.; Cornelissen, S.; Lagae, L.; Stakenborg, T.; van Dorpe, P. *Nat. Commun.* **2018**, *9*, 1733.
32. le Ru, E.C.; Etchegoin, P.G. *Annu. Rev. Phys. Chem.* **2012**, *63*, 65–87.
33. Yu, Y.; Xiao, T.H.; Wu, Y.; Li, W.; Zeng, Q.-G.; Long, L.; Li, Z.-Y. *Adv. Photonics* **2020**, *2*, 014002.
34. Fang, J.; et al. *Nano Lett.* **2010**, *10*, 5006–5013.
35. Zolotoukhina, T.; Yamada, M.; Iwakura, S. In Proceedings of the 1st International Electronic Conference on Biosensors (IECB 2020), 2–17 November 2020, p. 035671.
36. Zolotoukhina, T.; Yamada, M.; Iwakura, S. *Biosensors* **2021**, *11*, 37.
37. Cornell, W.D.; Cieplak, P.; Baryly, C.T.; Gould, I.R.; Merz, K.M., Jr.; Ferguson, F.M.; Spellmeyer, D.C.; Fox, T.; Caldwell, J.W.; Kollman, P.A. *J. Am. Chem. Soc.*, **1995**, *117*, 5179–5197.
38. Zayak, A.T.; Hu, Y.S.; Choo, H.; Bokor, J.; Cabrini, S.; Schuck, P.J.; Neaton, J.B. *Phys. Rev. Lett.* **2011**, *106*, 083003-1−083003-14.
39. Olsson, P.A.T. *J. App. Phys.* **2010**, *108*, 034318.
40. Wang, J.; Wang, G.; Zhao, J. *Chem. Phys. Lett.* **2003**, *380*, 716–720.
41. Lewis, L.J.; Jensen, P.; Combe, N.; Barrat, J.-L. *Phys. Rev. B* **2000**, *61*, 16084.
42. Latorre, F.; Kupfer, S.; Bocklitz, T.; Kinzel, D.; Trautmann, S.; Grafe, S.; Deckert, V. *Nanoscale* **2016**, *8*, 10229–10239.
43. Mante, P.-A.; Belliard, L.; Perrin, B. *Nanophotonics* **2018**, *7*, 1759–1780.
44. Shankla, M.; Aksimentiev, A. *ACS Appl. Mater. Interfaces* **2020**, *12*, 26624–26634.
45. Wanunu, M.; Sutin, J.; McNally, B.; Chow, A.; Meller, A. *Biophys. J.* **2008**, *95*, 4716–4725.